

# Materials Research Letters



ISSN: (Print) 2166-3831 (Online) Journal homepage: https://www.tandfonline.com/loi/tmrl20

# Creep properties of biodegradable Zn-0.1Li alloy at human body temperature: implications for its durability as stents

Suming Zhu, Chengcheng Wu, Guannan Li, Yufeng Zheng & Jian-Feng Nie

**To cite this article:** Suming Zhu, Chengcheng Wu, Guannan Li, Yufeng Zheng & Jian-Feng Nie (2019) Creep properties of biodegradable Zn-0.1Li alloy at human body temperature: implications for its durability as stents, Materials Research Letters, 7:9, 347-353, DOI: 10.1080/21663831.2019.1610106

To link to this article: <a href="https://doi.org/10.1080/21663831.2019.1610106">https://doi.org/10.1080/21663831.2019.1610106</a>

9	© 2019 The Author(s). Published by Informa UK Limited, trading as Taylor & Francis Group
	Published online: 09 May 2019.
	Submit your article to this journal $oldsymbol{oldsymbol{\mathcal{C}}}$
CrossMark	View Crossmark data 🗗





Check for updates

#### **ORIGINAL REPORT**

OPEN ACCESS

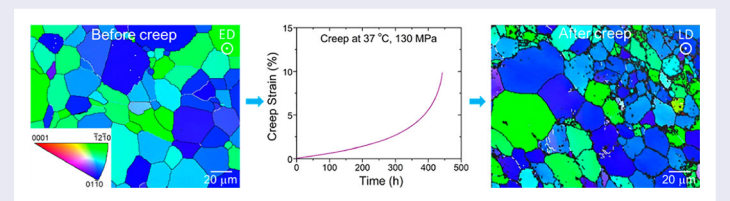
# Creep properties of biodegradable Zn-0.1Li alloy at human body temperature: implications for its durability as stents

Suming Zhu<sup>a</sup>, Chengcheng Wu<sup>a</sup>, Guannan Li<sup>b</sup>, Yufeng Zheng<sup>b</sup> and Jian-Feng Nie<sup>a</sup>

<sup>a</sup>Department of Materials Science and Engineering, Monash University, Clayton, Australia; <sup>b</sup>Department of Materials Science and Engineering, College of Engineering, Peking University, Beijing, People's Republic of China

#### **ABSTRACT**

This is the first report on creep properties of biodegradable zinc alloys at human body temperature. The extruded Zn-0.1Li (wt.%) alloy exhibits appreciable creep deformation at 37°C under stresses ranging 80–230 MPa within 500 h. The creep deformation at low stresses (80–155 MPa, about 0.4–0.8 yield strength) is characterized by a stress exponent of about 4 and an activation energy close to that for self-diffusion of zinc, which are typical of dislocation creep. The implications of creep at human body temperature for durability of biodegradable zinc alloys as stents are discussed.



#### **IMPACT STATEMENT**

This is the first report on creep properties of biodegradable zinc alloys at human body temperature. It is demonstrated that creep resistance is another crucial parameter in the design of biodegradable Zn alloys.

#### **ARTICLE HISTORY**

Received 23 January 2019

#### **KEYWORDS**

Biodegradable zinc alloys; creep properties; stress exponent; activation energy

# 1. Introduction

In recent years, zinc and its alloys have received increasing attention as a class of biodegradable materials due to their good biocompatibility and biodegradability [1]. Since pure Zn has poor mechanical properties that cannot meet the benchmark requirements for biomedical applications, i.e. yield strength > 200 MPa, ultimate tensile strength  $> 300 \,\mathrm{MPa}$ , elongation > 15-18% [2], the research efforts have been directed to enhancing the mechanical properties by alloying with other biocompatible elements, such as Li [3,4], Mg [5-8], Ca [8], Sr [8] and Cu [9,10]. Among the alloy systems investigated, Zn-Li is of interest because it is one of a few potentially agehardenable systems and the toxic potential is anticipated to be negligible [3,4]. The in vivo corrosion tests and in vivo biocompatibility tests [3,4] revealed that Zn-Li alloys had similar corrosion behaviour and biocompatibility to pure Zn.

A recent review [11] has summarized the latest progress in developing Zn alloys for vascular stent applications. It is noted that the alloy development and evaluation so far have been based on the tensile properties. corrosion behaviour and biocompatibility, with no creep resistance, especially at human body temperature, being taken into account. However, a stent needs to endure the radial pressure from the vessel for an extended period of time and insufficient creep resistance could result in its collapse or narrowing [12]. In fact, creep resistance has been an important consideration in evaluation of polymeric stent materials [13,14]. It has long been known that Zn, like other hcp metals such as Mg, Ti and Zr, tends to exhibit discernible creep at room temperature [15–17]. Room temperature creep has also been reported in Zn alloys, such as rolled Zn-(0.3-2.0)Cu alloys [18], rolled Zn-0.15Cu-0.07Ti alloy [19], extruded Zn-28.7Al-1.9Cu alloy [20] and die-cast Zn-4Al-(0-3Cu) alloys [21].

CONTACT Yufeng Zheng yfzheng@pku.edu.cn Department of Materials Science and Engineering, College of Engineering, Peking University, Beijing 100871, People's Republic of China; Jian-Feng Nie jianfeng.nie@monash.edu Department of Materials Science and Engineering, Monash University, Clayton, Victoria 3800, Australia

In most cases, self-diffusion controlled dislocation creep was suggested to be the dominant deformation mechanism. For example, Kallien et al. [21] studied the creep properties of die-cast Zn-4Al-(0-3Cu) alloys at 25-85°C and obtained a stress exponent of 4-5 and an activation energy of about 94 kJ/mol. It is thus expected biodegradable Zn alloys could undergo creep deformation at room temperature and, needless to say, human body temperature.

This paper reports the creep properties of a biodegradable Zn alloy, Zn-0.1Li at 37°C, a typical human body temperature, over stresses ranging 80-230 MPa. To the best of the authors' knowledge, this is the first report on creep properties of biodegradable Zn alloys at human body temperature.

# 2. Experimental methods

The Zn-0.1Li alloy in this work was prepared from high purity pure Zn and a Zn-5Li master alloy. The raw materials were melted in a high purity graphite crucible under the protection of mixed gas of SF<sub>6</sub> (1 vol.%) and CO<sub>2</sub> (balance). After being held at 480°C for 30 min, the melt was poured into a steel mould that was preheated to 150°C. Cylindrical blocks of 40 mm in diameter were cut from the ingot and were extruded at 300°C into billets of 10 mm in diameter (extrusion ratio 16:1). From the extruded billets, cylindrical specimens with a gauge length of 16 mm and a diameter of 3.5 mm were machined for creep testing. The constant-load tensile creep tests were carried out on self-designed creep testing rigs, equipped with silicone oil baths. The specimens were immersed into the heated oil baths, with the temperature controlled to within  $\pm 1$ °C. Most creep tests were conducted at 37°C, a typical human body temperature; some tests were conducted at 23°C and 51°C in

order to determine the temperature dependence of creep properties. The tests were run until failure of specimens or interrupted after 500 h. Tensile tests were also carried out at room temperature on a screw-driven Instron machine at a crosshead speed of 1 mm/min, corresponding to an initial strain rate of  $1 \times 10^{-3}$  s<sup>-1</sup>. Microstructures before and after creep testing were characterized by scanning electron microscopy (SEM), couple with electron backscatter diffraction (EBSD), using a JEOL 7001 FEG SEM equipped with an Aztec analysis system. The EBSD samples were prepared by electropolishing in a solution containing 5.3 g lithium chloride, 11.16 g magnesium perchlorate, 500 ml methanol and 100 ml 2-butoxy-ethanol at 100 V and −45°C. The dislocation substructure developed in the crept specimens was characterized by transmission electron microscopy (TEM) in a Tecnai G2 T20 microscope. The TEM foils were prepared by low-angle ion milling using Gatan Precision Ion Polishing System (PIPS) with a cold stage to prevent any microstructural evolution.

#### 3. Results and discussion

The SEM micrograph and EBSD orientation map of the as-extruded Zn-0.1Li alloy are shown in Figure 1(a,b), respectively. The microstructure consists of equiaxed grains and stringers of intermetallic phase (presumably LiZn<sub>4</sub>) aligned along the extrusion direction (Figure 1(a)), indicating that the grains have fully recrystallized after the extrusion. There appears a bi-modal grain size distribution, with the fine grains being associated with the stringers of particles. The bi-modal grain structure is also confirmed by the EBSD map (Figure 1(b)), where there is a mixture of fine grains and relatively large ones. An average grain size of  $\sim$  26 µm is obtained from the EBSD map. It is noted that the alloy

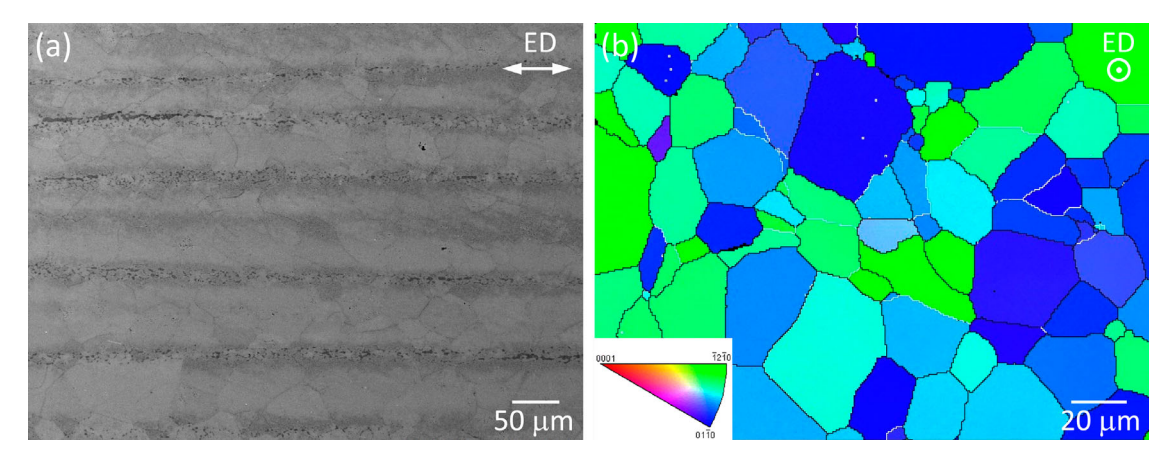


Figure 1. Microstructure in the as-extruded Zn-0.1Li alloy: (a) SEM secondary electron image showing grain structure and stringers of intermetallic phase along the extrusion direction (ED) and (b) EBSD orientation map and inverse pole figure perpendicular to ED. The white lines in (b) indicate low angle grain boundaries.

**Table 1.** Tensile properties of the extruded Zn-0.1Li alloy at room temperature. The data for a similar alloy from literature are also shown for comparison.

Sample	Yield Strength (MPa)	Tensile Strength (MPa)	Elongation (%)
This work Zhao et al. [3]	$189.1 \pm 4.7$ $238 \pm 60$	$230.2 \pm 0.4$ $274 \pm 61$	4.0 ± 0.6 17 ± 7

has a typical (0001) fibre texture, with the *c*-axis of most grains aligned perpendicular to the extrusion direction.

The tensile properties of the extruded Zn-0.1Li alloy at room temperature are listed in Table 1. Also shown are room temperature tensile properties reported by Zhao et al. [3] for a similar alloy. It is noted that the current alloy has much lower strength properties than the alloy in Ref. [3]. Such differences in strength properties are considered to be due to the different deformation processing conditions.

The creep curves of the Zn-0.1Li alloy tested at 37°C under various stresses are shown in Figure 2(a) while

the creep curves at different temperatures under constant stress of 130 MPa are shown in Figure 2(b). The alloy exhibits substantial creep deformation for the applied stresses from 80 to 230 MPa. Even for the lowest stress level (80 MPa, about 0.4 yield strength), a strain of  $\sim 0.57\%$  is generated after 500 h. The creep deformation is apparently affected by changing the test temperature (Figure 2(b)). It is worth noting that the alloy even shows appreciable creep deformation at room temperature (23°C) with a stress of 130 MPa (about 0.7 yield strength). These results indicate clearly that creep is an issue for Zn alloys at human body temperature.

The creep curves in Figure 2(a,b) exhibit typical threestage creep behaviour, i.e. the primary stage in which the creep rate decreases with increasing creep time, the secondary stage in which the creep rate remains steady and the tertiary stage in which the creep rate increases with time until fracture. It is noted that, however, the secondary stage is very limited for the Zn-0.1Li alloy; after a minimum value is reached, the creep rate tends to

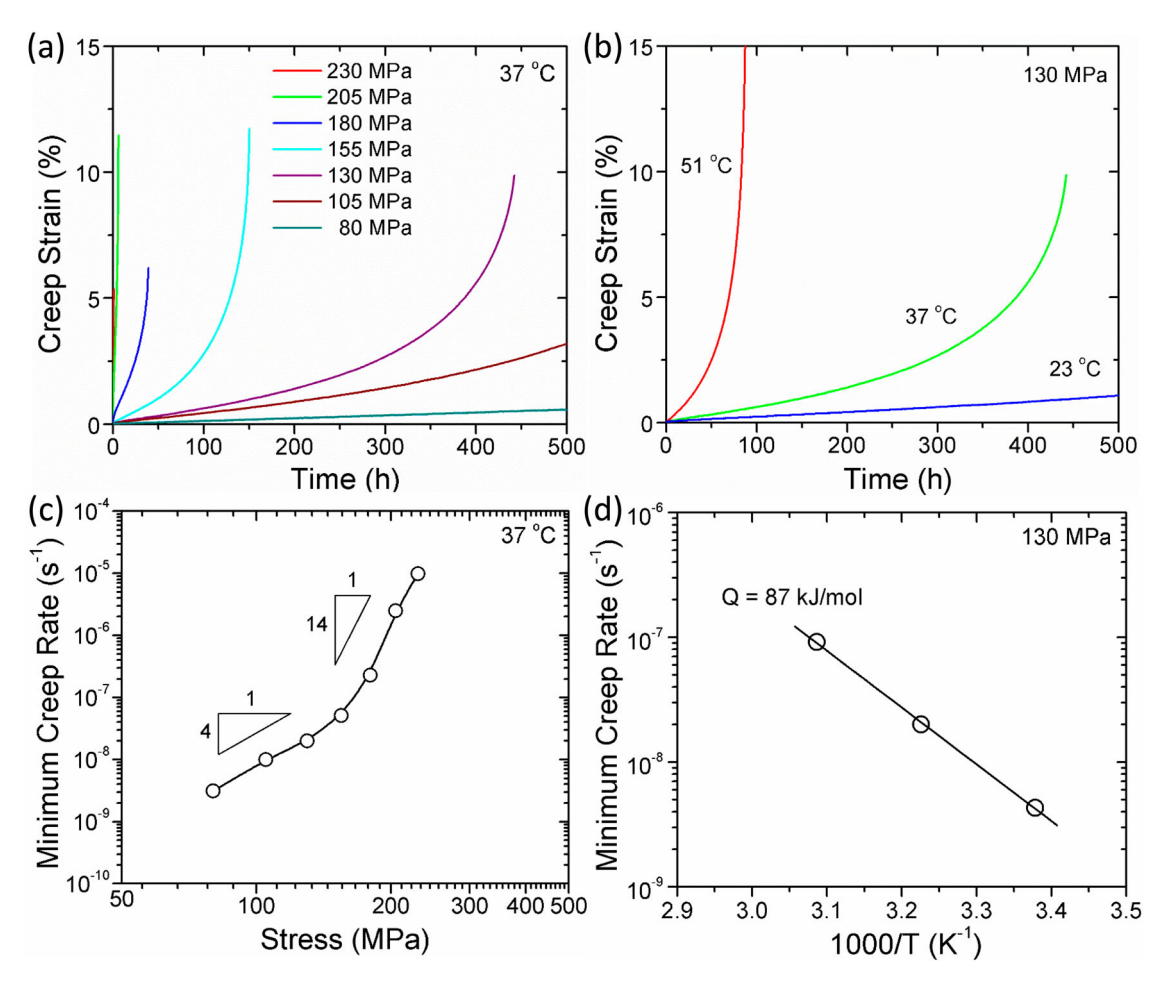


**Figure 2.** Creep behaviour of the Zn-0.1Li alloy: (a) creep curves under various stresses at 37°C, (b) creep curves at different temperatures under a constant stress of 130 MPa, (c) the minimum creep rate plotted against the applied stress at 37°C and (d) the minimum creep rate plotted against reciprocal of temperature for a constant stress of 130 MPa.

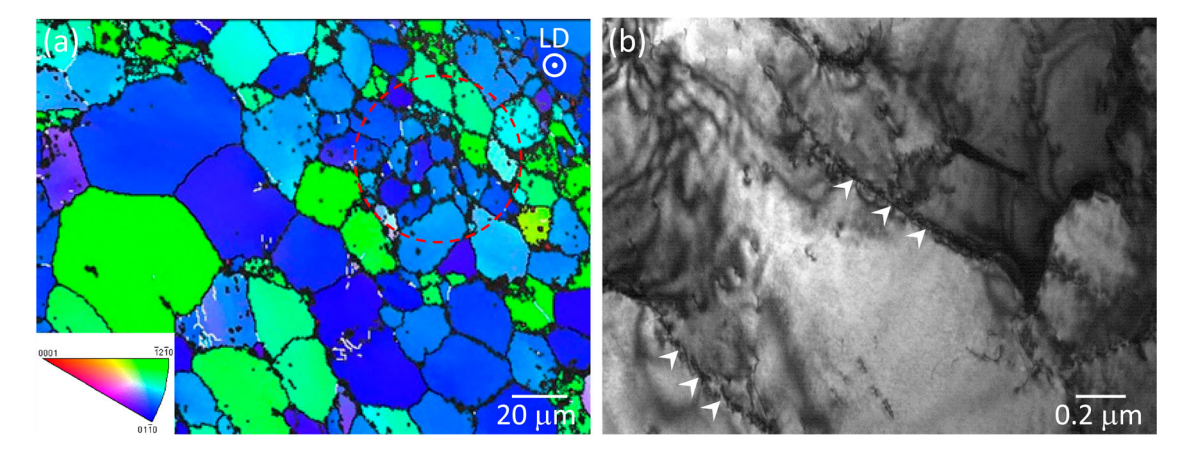


**Figure 3.** Microstructure in the Zn-0.1Li alloy after creep at  $37^{\circ}$ C and  $130 \, \text{MPa}$  to a strain of  $\sim 0.03$ : (a) EBSD orientation map and inverse pole figure and (b) TEM micrograph, both perpendicular to the loading direction (LD). The white lines in (a) indicate low angle grain boundaries and the red circle indicates small grains from dynamic recrystallization. The white arrows in (b) indicate the subgrain boundaries.

increase progressively over the most creep duration. This kind of creep behaviour is termed as 'extended period of tertiary creep' [22]. Therefore, the minimum creep rate,  $\dot{\varepsilon}_m$  is used instead of the steady-state creep rate to correlated with the applied stress,  $\sigma$ , and the test temperature, T, by a power-law equation of the form

$$\dot{\varepsilon}_m = A\sigma^n exp(-Q_c/RT),\tag{1}$$

where A is a material-dependent constant, n the stress exponent, Qc the activation energy and R the gas constant. Plots of the minimum creep rate against the applied stress and reciprocal of temperature using double logarithmic coordinates are shown in Figure 2(c,d), respectively. The stress exponent, computed from the plot in Figure 2(c), appears to vary with the applied stress, increasing from  $\sim 4$  at low stresses to  $\sim 14$  at high stresses, suggesting a transition from power-law regime to power-law breakdown regime with increasing stress [23]. The activation energy, determined from the plot in Figure 2(d), is 87 kJ/mol for creep at the low stresses. This value is close to that for the lattice self-diffusion of Zn, which is 92 kJ/mol [24]. The above results indicate that the predominant creep mechanism of the Zn-0.1Li alloy at low stresses is most likely dislocation creep that is controlled by the lattice self-diffusion of Zn.

The EBSD and TEM analyses of the microstructure and dislocation substructure developed in the Zn-0.1Li alloy after creep at 130 MPa to a strain of  $\sim 3\%$  are shown in Figure 3. As compared with the orientation map before creep (Figure 1(b)), some distinct changes can be noted in the orientation map in Figure 3(a). Firstly, there are faint colour differences and low angle grain boundaries within grains, indicating the development of in-grain misorientations. Secondly, there appears

small grains with large orientation deviations, suggesting the occurrence of dynamic recrystallization. Thirdly, some grain boundaries, especially the triple junctions are undistinguishable by EBSD, indicating that the creep deformation is highly concentrated in these areas. Formation of well-defined subgrains is also evidenced by TEM (Figure 3(b)). These recovery-related microstructural features are in support of the dislocation dominated creep mechanism as stated.

The creep rupture properties of the Zn-0.1Li alloy at 37°C are presented in Figure 4. As can be expected, the rupture time decreases with an increase in the applied stress. Moreover, the rupture time,  $t_r$ , can be correlated well with the minimum creep rate by the empirical Monkman-Grant equation [25]

$$t_r \cdot \dot{\varepsilon}_m = C, \tag{2}$$

where *C* is a material-dependent constant. This suggests that the creep rupture of the Zn-0.1Li alloy is fully controlled by the creep deformation. The SEM examinations of the longitudinal section and the fracture surface of the specimen tested to failure at 130 MPa are shown in Figure 5. There is extensive creep cavitation developed in the specimen, especially near the fracture surface. Most cavities appear to locate at grain boundaries, especially at tripe junctions. Despite the extensive creep cavitation at grain boundaries, however, the final fracture appears to be a mixture of intergranular and transgranular modes, with both cavitation and dimple-like features being visible. Similar cavitation has been reported in fine-grained Zn-22Al alloy within the superplastic range and at lower strain rates [26,27].

The creep damage tolerance parameter, defined as  $\lambda = \varepsilon_r/(t_r \cdot \dot{\varepsilon}_m)$  ( $\varepsilon_r$  is the rupture strain) by Ashby and Dyson [28], is usually used to describe the tolerance

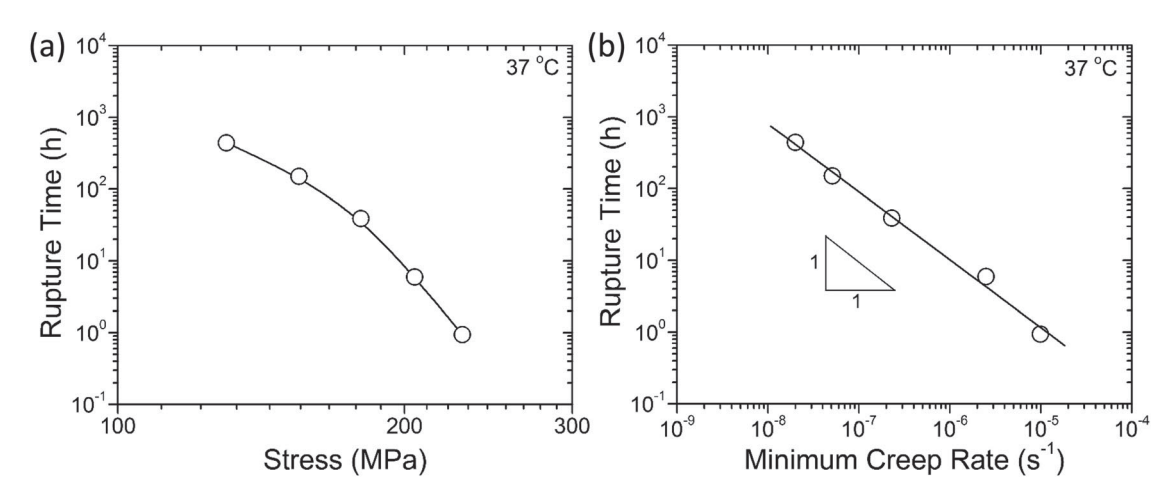


**Figure 4.** Creep rupture behaviour of the Zn-0.1Li alloy at 37°C: (a) the rupture time plotted against the applied stress and (b) correlation between the rupture time and the minimum creep rate.

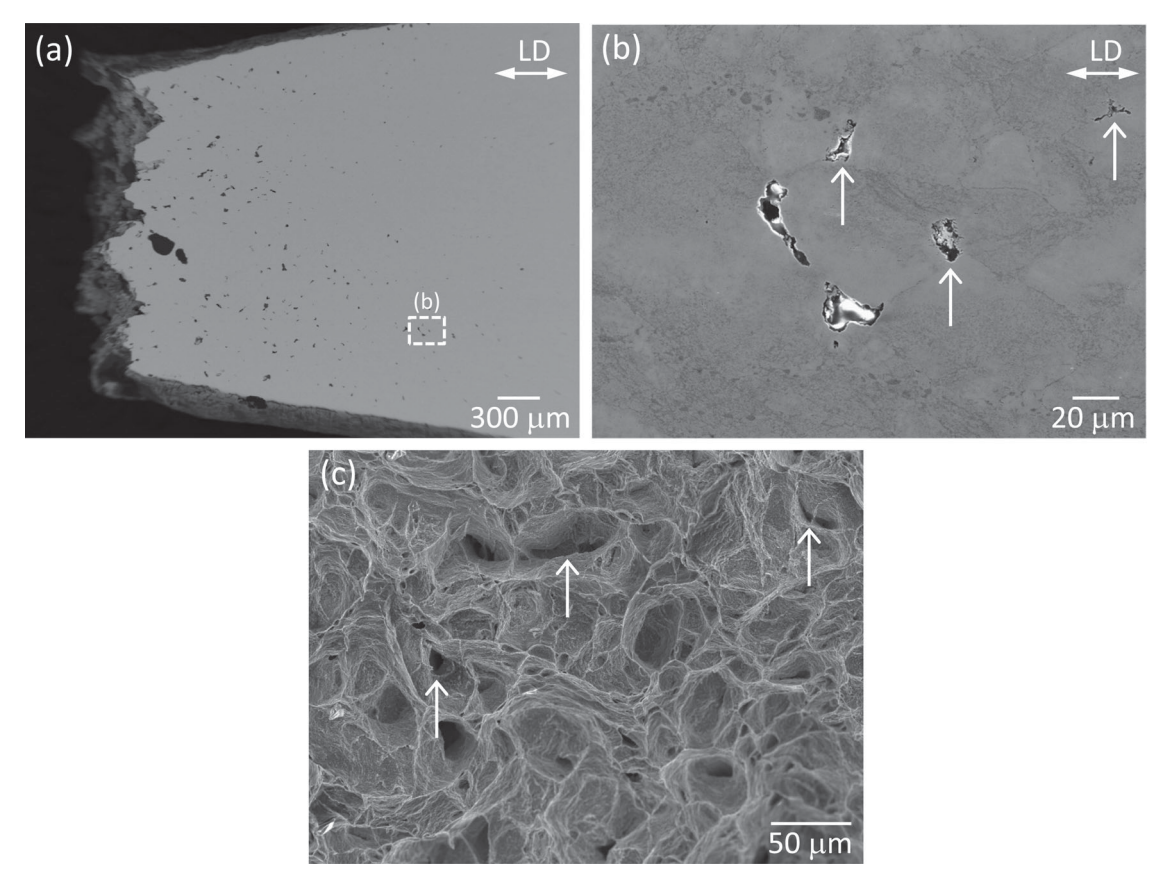


**Figure 5.** SEM observations of the specimen tested to failure at 37°C under 130 MPa: (a) backscattered electron image showing the longitudinal section near the fracture surface (loading direction is horizontal), (b) secondary electron image showing an enlarged area in (a), and (c) secondary electron image showing a top view of the fracture surface. The arrows in (b) and (c) indicate cavities developed during creep.

of a material to local strain concentration and to provide an indication of the underlying damage mechanism that is responsible for tertiary creep and final fracture. According to Ashby and Dyson [28], for materials with  $\lambda=1-2.5$  tertiary creep results from intergranular cavitation and brittle intergranular fracture is expected.

For materials with higher values of  $\lambda$ , tertiary creep is dominated by mechanical instability due to necking ( $\lambda > 2.5$ ) or microstructural degradation due to coarsening of precipitate particles or recovery of dislocation substructure ( $\lambda > 5$ ), and ductile transgranular (dimple) fracture becomes the dominant fracture mode. For the

Zn-0.1Li alloy, the  $\lambda$  value is between 3 and 4 at low stresses, suggesting that necking could be the dominant creep damage mechanism. Given that extensive creep cavitation at grain boundaries is evidenced in the fractured specimen, the fracture of the Zn-0.1Li alloy is probably caused by necking coupled with creep cavitation, a mechanism suggested by Skleničkain for the creep fracture of tempered martensitic 9%Cr steel [29]. However, since necking normally leads to conventional tertiary creep just as creep cavitation does, the extended tertiary creep in the Zn-0.1Li alloy is believed to be most likely result from the recovery of dislocation substructure, as evidenced by the occurrence of dynamic recrystallization during creep process (Figure 3).

One primary requirement for biodegradable vascular stents is mechanical integrity for the first 3-6 months within a life time of 12-24 months [2,11]. For balloon expandable stents, the alternate stress for the worst-case location was computed to be 48 MPa at 100 mm Hg by Marrey et al. [30], 52 MPa at 100 mm Hg by Xu et al. [31] and 38.2 MPa/57.3 MPa at 80/120 mm Hg by Xuan et al. [32]. Given that appreciable creep deformation ( $\sim 0.57\%$ ) is evidenced for the Zn-0.1Li alloy at 37°C for a stress down to 80 MPa (about 0.4 yield strength) after 500 h ( $\sim$ 0.25 of the minimum duration required for mechanical integrity of stents), creep at human body temperature is expected to have an adverse effect on the durability of this alloy as biodegradable stents. It is thus suggested that creep at human body temperature should not be neglected for Zn alloys developed for biodegradation applications.

#### 4. Conclusions

The creep and rupture properties of biodegradable Zn-0.1Li alloy at human body temperature have been studied. The alloy exhibits appreciable creep deformation at 37°C even for a stress as low as about 0.4 yield strength. There is a transition from power-law dislocation creep to power-law breakdown with increasing stress. The creep at low stresses is characterized by a stress exponent of about 4 and an activation energy close to that for selfdiffusion of Zn. Although extensive creep cavitation is developed at grain boundaries, the final fracture is a mixture of intergranular and transgranular modes. The present work suggests that creep resistance at human body temperature should be taken into account in the development of biodegradable zinc alloys.

# **Acknowledgements**

C. Wu wishes to acknowledge the Australian Postgraduate Award and International Postgraduate Research Scholarship.

Monash Centre for Electron Microscopy (MCEM) is acknowledged for access to experimental facilities.

## **Disclosure statement**

No potential conflict of interest was reported by the authors.

## **Funding**

This work was supported by Australian Research Council (ARC) through Discovery grant DP190102373 and National Natural Science Foundation of China (grant number 51431002).

#### References

- [1] Bowen PK, Drelich J, Goldman J. Zinc exhibits ideal physiological corrosion behavior for bioabsorbable stents. Adv Mater. 2013;25:2577-2582.
- [2] Werkhoven RJ, Sillekens WH, van Lieshout JBJM. Processing aspects of magnesium alloy stent tube. In: Sillekens WH, Agnew SR, Neelameggham NR, Mathaudhu SN, editor. Magnesium technology 2011. Cham: Springer; 2016. p. 419-424.
- [3] Zhao S, Seitz J-M, Eifler R, et al. Zn-Li alloy after extrusion and drawing: structural, mechanical characterization, and biodegradation in abdominal aorta of rat. Mater Sci Eng C. 2017;76:301-312.
- [4] Zhao S, McNamara CT, Bowen PK, et al. Structural characteristics and in vitro biodegradation of a novel Zn-Li alloy prepared by induction melting and hot rolling. Metall Mater Trans A. 2017;48:1204-1215.
- [5] Vojtech D, Kubasek J, Serak J, et al. Mechanical and corrosion properties of newly developed biodegradable Zn-based alloys for bone fixation. Acta Biomater. 2011;7:3515-3522.
- [6] Jin H, Zhao S, Guillory R, et al. Novel high-strength, lowalloys Zn-Mg ( < 0.1 wt% Mg) and their arterial biodegradation. Mater Sci Eng C. 2017;84:67-79.
- [7] Mostaed E, Sikora-Jasinska M, Mostaed A, et al. Novel Zn-based alloys for biodegradable stent applications: design, development and in vitro degradation. J Mech Behav Biomed Mater. 2016;60:581-602.
- [8] Li HF, Xie XH, Zheng YF, et al. Development of biodegradable Zn-1X binary alloys with nutrient alloying elements Mg, Ca and Sr. Sci Rep. 2015;5:10719.
- [9] Niu J, Tang Z, Huang H, et al. Research on a Zn-Cu alloy as a biodegradable material for potential vascular stents application. Mater Sci Eng. C. 2016;69:407-413.
- [10] Tang Z, Niu J, Huang H, et al. Potential biodegradable Zn-Cu binary alloys developed for cardiovascular implant applications. J Mech Behav Biomed Mater. 2017;72:182-191.
- [11] Mostaed E, Sikora-Jasinska M, Drelich JW, et al. Zincbased alloys for degradable vascular stent applications. Acta Biomater. 2018;71:1-23.
- [12] Kimble LD, Bhattacharyya D, Fakirov S. Biodegradable microfibrillar polymer-polymer composites from poly(L-lactic acid)/poly(glycolic acid). Express Polym Lett. 2015;9:300-307.
- [13] Pietrzak WS. Creep analysis of PLLA: PGA copolymer craniofacial plates. J Craniofac Surg. 2012;23:1507-1512.



- [14] Kimble LD, Bhattacharyya D. In vitro degradation effects on strength, stiffness, and creep of PLLA/PBS: a potential stent material. Int J Polym Mater Po. 2015;64:299-310.
- [15] Cottrell AH, Aytekin V. Andrade's creep law and the flow of zinc crystals. Nature. 1947;160:328-329.
- [16] Matsunaga T, Kameyama T, Takahashi K, et al. Constitutive relation for ambient-temperature creep in hexagonal close-packed metals. Mater Trans. 2009;50:2858-2864.
- [17] Matsunaga T, Kameyama T, Takahashi K, et al. Intragrandeformation mechanisms during ambienttemperature creep in hexagonal close-packed metals. Mater Trans. 2009;50:2865-2872.
- [18] Sharma RC, Martin JW. Creep of dilute zinc-copper alloys. J Mater Sci. 1974;9:1139-1144.
- [19] Quintana MJ, García JO, González R, et al. Influence of strain rate and heat treatments on tensile and creep properties of Zn-0.15Cu-0.07Ti alloys. DYNA. 2016;83:77-83.
- [20] Muñoz-Andrade JD, Mendoza-Allende A, Cabrera E, et al. Effect of grain size on the activation energy for plastic deformation near room temperature in a Zn-28.7 pct Al-1.9 pct Cu alloy. J Mater Sci. 2007;42:7617-7620.
- [21] Kallien LH, Leis W. Ageing of zink alloys. Int Foundry Res. 2011;64(1):2-23.
- [22] Dyson BF, Gibbons TB. Tertiary creep in nickel-base superalloys: analysis of experimental data and theoretical synthesis. Acta Metall. 1987;359:2355-2369.
- [23] Sherby OD, Burke PM. Mechanical behavior of crystalline solids at elevated temperature. Prog Mater Sci. 1968;13:323-390.
- [24] Frost HJ, Ashby MF. Deformation-mechanism maps: the

- plasticity and creep of metals and ceramics. New York: Pergamon Press; 1982.
- [25] Monkman FC, Grant NJ. An empirical relationship between rupture life and minimum creep rate in creeprupture tests. Proc ASTM. 1956;56:593-620.
- [26] Ishikawa H, Bhat DG, Mohamed FA, et al. Evidence for cavitation in the superplastic Zn-22 pct Al eutectoid. Metall Trans A. 1977;8:523-525.
- [27] Park K-T, Mohamed FA. Effect of impurity content on cavitation in the superplastic Zn-22 pct Al alloy. Metall Trans A. 1990;21:2605-2608.
- [28] Ashby MF, Dyson BF. Creep damage mechanics and micromechanisms. In: Valluri SR, Taplin DMR, Rao PR, Knott JF, Dubey R, editor. Fracture 84. New York: Pergamon Press; 1984. p. 3-30.
- [29] Sklenicka V, Kucharova PK K, Kvapilova M, et al. Applicability of empirical formulas and fractography for assessment of creep life and creep fracture modes of tempered martensitic 9%Cr steel. Kov Mater. 2017;55:
- [30] Marrey RV, Burgermeister R, Grishaber RB, et al. Fatigue and life prediction for cobalt-chromium stents: a fracture mechanics analysis. Biomater. 2006;27:1988-2000.
- [31] Xu J, Yang J, Huang N, et al. Mechanical response of cardiovascular stents under vascular dynamic bending. Biomed Eng Online. 2016;15:21.
- [32] Xuan Y, Dvir D, Wang Z, et al. Stent and leaflet stresses in 26-mm, third-generation, balloon-expandable transcatheter aortic valve. J Thorac Cardiovasc Surg. 2019;157:528-536.